Thickness dependence of microstructures in $La_{0.8}Ca_{0.2}MnO_3$ thin films

H. D. Zhang,[a] M. Li, Y. K. An, and Z. H. Mai
Beijing National Laboratory for Condensed Matter Physics, Institute of Physics, Chinese Academy of Sciences, Beijing 100080, People's Republic of China

J. Gao and F. X. Hu
Department of Physics, The University of Hong Kong, Pokfulam Road, Hong Kong, People's Republic of China

Y. Wang and C. J. Jia
Beijing Synchrotron Radiation Facility, Institute of High Energy Physics, Chinese Academy of Sciences, Beijing 100049, People's Republic of China

(Received 29 November 2005; accepted 25 April 2006; published online 10 July 2006)

The thickness dependence of microstructures of $La_{0.8}Ca_{0.2}MnO_3$ (LCMO)/$SrTiO_3$ (STO) thin films was investigated by high-resolution x-ray diffraction, small angle x-ray reflection, grazing incidence x-ray diffraction, scanning electron microscopy, and atomic force microscopy. The results show that all the LCMO films are well oriented in (00*l*) direction perpendicular to the substrate surface. Self-organized crystalline grains with a tetragonal shape are uniformly distributed on the film surface, indicating the deposition condition being of benefit to the formation of the crystalline grains. With increasing the film thickness, the crystalline quality of the LCMO film is improved, while the surface becomes rougher. There exists a nondesigned cap layer on the upper surface of the LCMO layer for all the samples. The mechanism is discussed briefly. © *2006 American Institute of Physics*. [DOI: 10.1063/1.2210147]

I. INTRODUCTION

Manganite perovskite thin films possess many particularly properties, such as superconductivity,[1–3] colossal magnetoresistance (CMR),[4,5] ferroelectricity,[6,7] dielectricity, etc. CMR manganite perovskite thin films ($RE_{1-x}A_xMnO_3$) currently are a focus of active research because of their potential application in magnetic sensors, high-speed high-density memory devices, and optoelectronic devices.[8–10] Manganite $La_{1-x}Ca_xMnO_3$ materials exhibit a very large magnetoresistance effect at the temperature close to ferromagnetic-paramagnetic transition. In $La_{1-x}Ca_xMnO_3$ systems, there exist rich structural phases with variations of x (Ca^{2+} concentration).[11] $La_{0.8}Ca_{0.2}MnO_3$ has an orthorhombic distorted perovskite structure. This reduction in symmetry compared to the ideal cubic perovskite is mainly due to Jahn-Teller distortion of the O_6 octahedron surrounding the Mn ions. The little change in the local atom arrangement would affect the hopping amplitudes of the e_g electrons via oxygen $2p$ states qualitatively which is the double-exchange mechanism.[12] The occurrence of CMR behavior and magnetic properties with film thickness is attributed to the presence of the lattice strain and the disorder in epitaxial films. The effect of thickness of LCMO thin film on the microstructures and the strain distribution inside the films is an important parameter for potential device applications. The different thickness of thin films can be used by film epitaxial growth to tailor biaxial epitaxial strain.[13–15] Varying the film thickness can control the magnetic anisotropy and other strain dependent properties.

In order to study the structural dependence of magnetic and electrical transport properties of the film, it is essential to characterize both surface and interface structure of strained films with varying thickness. In this paper we report the thickness dependence of the microstructures and the surface morphology of $La_{0.8}Ca_{0.2}MnO_3$ films grown on $SrTiO_3$ substrates investigated by x-ray techniques, scanning electron microscopy (SEM), and atomic force microscopy (AFM).

II. EXPERIMENTS

Thin films of $La_{0.8}Ca_{0.2}MnO_3$ (LCMO) with different film thickness were deposited on (100) $SrTiO_3$ (STO) substrates using pulsed laser deposition technique.[16] In brief, the chamber was evacuated to a pressure less than 6×10^{-6} mbar before the deposition. The deposition took place in a pure oxygen gas of the pressure of 0.1 mbar. The substrate temperature was kept at 750 °C during the deposition. The energy of laser beam is ~280 mJ, the wavelength is 308 nm, and the pulse frequency is 4 Hz. The thickness of thin films is controlled by the deposition time. In order to avoid oxygen deficiency, the as-grown films were annealed at 800 °C for 1 h in air after deposition. To investigate the effect of the thickness of LCMO layers on the microstructures, five samples were prepared with the LCMO film thickness of 10, 20, 40, 70, and 100 nm, labeled A, B, C, D, and E, respectively.

The high-resolution x-ray diffraction and the x-ray small angle reflection measurements were performed on a high-resolution x-ray diffractometer (Bruker D8 Advance) at room temperature with Cu $K\alpha_1$ radiation. The incidence slit is 0.1 mm and the detector slit is 0.2 mm. The experimental

[a]Author to whom correspondence should be addressed; FAX: +86-10-82640224; electronic mail: candy002_zhd@yahoo.com.cn

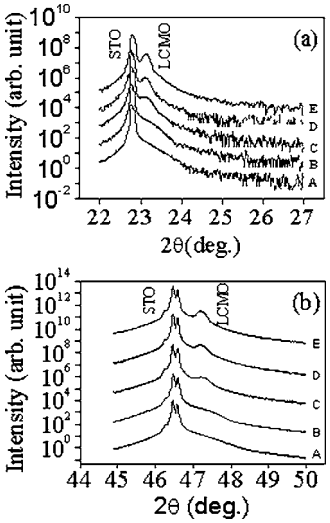

FIG. 1. X-ray diffraction profiles of samples A–E. (a) (001) diffraction of STO and LCMO. (b) (002) diffraction of STO and LCMO.

data of reflectivity were simulated theoretically using matrix formulation based on Fresnel's law in classical optics.[17,18]

The grazing incidence x-ray diffractions (GIXRDs) were measured at the Diffuse Scattering Station on the 4W1C beam line in the Beijing Synchrotron Radiation Facility (BSRF). The electron energy was 2.2 GeV and x-ray wavelength of 1.546 Å was used. The beam size was confined by a slit of dimension 0.2×1 mm^2. The energy resolution $\Delta E/E$ is about 4×10^{-4}. A slit of 1 mm wide was positioned before the sample and an ion chamber behind the slit was used to monitor the intensity of the incident beam. A NaI scintillator behind the diffraction slit of 0.2 mm wide was used to collect the reflected/scattered intensity from the sample. The ratio of counting coefficients of the two detectors was calibrated by measuring the incident x-ray beam intensity directly without the sample.

The surface morphology of the films was characterized by AFM on a NanoScope IIIa scanning probe microscope (DI Company, USA) in contact mode and SEM on a Hitachi S-4200 scanning electron microscope.

III. RESULTS AND DISCUSSIONS

A. The orientation and the lattice constants

Figure 1 shows the high-resolution x-ray diffraction profiles of the five samples. It is evident that only (00*l*) diffraction peaks of LCMO and STO are observed without diffraction peaks due to random crystallographic orientation or secondary phases. This suggests that the LCMO layers are *c*-axis oriented and highly epitaxial growth perpendicular to the substrate surface. From Fig. 1 it can also be found that the full width at half maximum (FWHM) of the (002) LCMO peak of samples A–D and E becomes narrow, indicating the crystalline quality of the samples being better with the thickness increasing. The out-of-plane lattice parameters of LCMO layers are determined by their diffraction peak positions, as shown in Fig. 2. One can see from Fig. 2 that with the thickness of the LCMO film increasing its out-of-plane lattice parameter *c* increases. And then the values of *c*

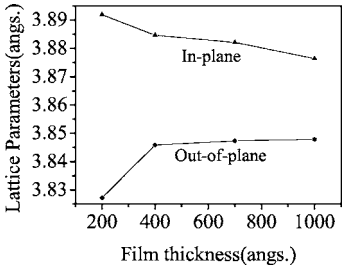

FIG. 2. Effect of thickness on the lattice parameters *c* and *a* of epitaxial LCMO films.

tend to a saturated value. To obtain in-plane lattice parameter grazing incidence x-ray diffractions were performed. Figure 3 shows the grazing incidence x-ray (020) diffraction profiles of samples B and E. One can see that on the lower incidence angle curves there are two diffraction peaks corresponding to the substrate and the LCMO films, respectively. With increasing the incidence angle the intensity of the film peak decreases. The behavior of grazing incidence x-ray (020) diffraction profiles for the other samples is very similar to that of Fig. 3. According to the position of the film peak, the in-plane lattice parameter is obtained. The in-plane lattice parameters of the samples are also shown in Fig. 2. As well known the lattice parameter of STO substrate is $a=3.905$ Å. Therefore, the LCMO film undergoes an in-plane tensile stress leading to a smaller lattice parameter *c* due to the tetragonal distortion. The LCMO thin film is a distorted perovskite with a pseudocubic. As film thickness increases, the in-plane lattice parameters decrease and out-of-plane lattice parameter increases.

B. Surface and interface roughness

To investigate the surface and interface structure of the LCMO films, x-ray small angle reflection was performed on the five samples. As well known small angle reflectivity is a sensitive technique to measure the chemical compositions of each layer in multilayers to investigate microstructures per-

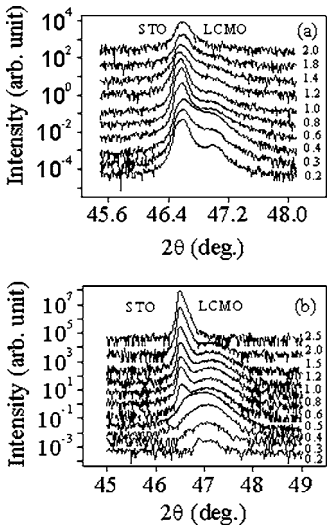

FIG. 3. The grazing incidence x-ray (020) diffraction profiles of STO and LCMO. (a) Sample B and (b) sample E.

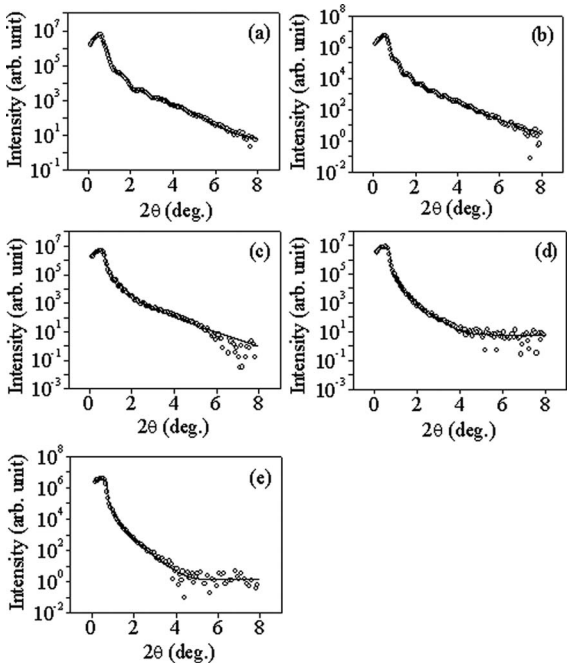

FIG. 4. X-ray reflectivity profiles of samples A–E. Circle represents experiment curve and solid line represents fitting curve.

pendicular to the surface such as the electron density, thickness, interface roughness, etc., by the theoretical simulation of the experimental data. Figure 4 shows the experimental and theoretical profiles of the x-ray small angle reflectivity of the five samples, respectively. From Fig. 4 one can see that the theoretical curves fit the experimental curves well. And the interdistance of the diffraction peaks decreases while the peak number increases with increasing the film thickness. Through simulating the experimental results, the atomic density, the thickness of each layer, and the roughness (rms) of the interface and the surface of the LCMO layer will be obtained. The best fitting parameters of the theoretical simulations are listed in Table I. It is clear from Table I that the nominal thickness of LCMO layer for all samples deviates slightly from the real thickness. It might be caused by fluctuations of deposition condition during the preparation of the films. With the film thickness increasing, the surface roughness increases. This result is in agreement with that of AFM (as shown in Fig. 5). A larger roughness on the surface than that at the interface might be due to high-energy particle bombardment during deposition process, which enabled the atoms on the surface to migrate or bond. As a result, crystalline grains grow up on the surface of the LCMO layer with the thickness increasing observed by SEM in the next section. One can note that there exists a nondesigned cap layer on the upper surface of the LCMO film which was also discovered in LCMO (Ref. 19) and PZT (Ref. 20) systems. The thickness of the cap layer increases with the thickness of the LCMO film because the thicker the LCMO film, the longer the depositing time. These nondesigned cap layers might be caused by oxidation on the top surface.

TABLE I. Theoretical simulation results of the small angle reflection curves.

Sample	Layer	Thickness (±2 Å)	Density (± 0.001 at./Å^3)	Surface and interface roughness (±1 Å)
	Cap layer	19	0.066	$\sigma_{air/cap}=3$
A	LCMO	72	0.086	$\sigma_{cap/LCMO}=4$
	STO	···	0.084	$\sigma_{LCMO/STO}=6$
	Cap layer	30	0.026	$\sigma_{air/cap}=20$
B	LCMO	144	0.086	$\sigma_{cap/LCMO}=3$
	STO	···	0.084	$\sigma_{LCMO/STO}=6$
	Cap layer	55	0.057	$\sigma_{air/cap}=40$
C	LCMO	310	0.096	$\sigma_{cap/LCMO}=3$
	STO	···	0.084	$\sigma_{LCMO/STO}=11$
	Cap layer	65	0.074	$\sigma_{air/cap}=45$
D	LCMO	632	0.096	$\sigma_{cap/LCMO}=6$
	STO	···	0.084	$\sigma_{LCMO/STO}=14$
	Cap layer	70	0.076	$\sigma_{air/cap}=55$
E	LCMO	900	0.096	$\sigma_{cap/LCMO}=6$
	STO	···	0.084	$\sigma_{LCMO/STO}=16$

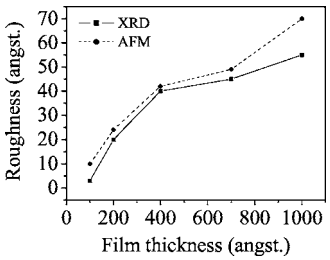

FIG. 5. The dependence of the surface roughness on the film thickness.

C. Surface morphology

Figure 6 shows the SEM images of samples A–E. One can see that the surface morphology of the films strongly depends on the thickness. (1) There exist self-organized crystalline grains with a tetragonal shape uniformly distributed

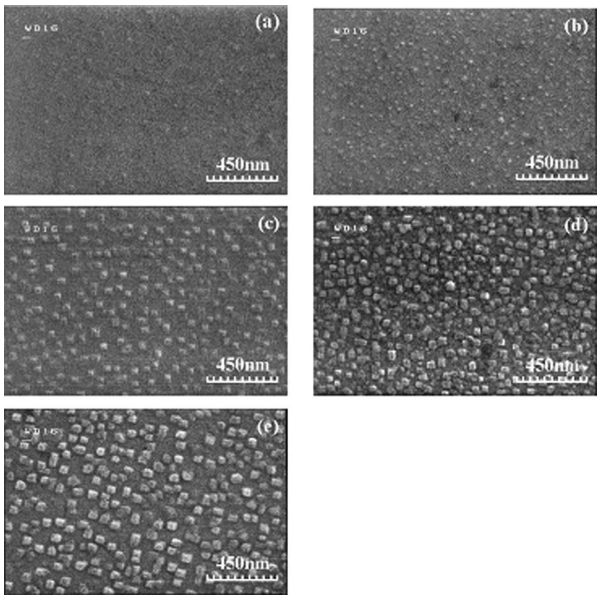

FIG. 6. The SEM images of samples A–E.

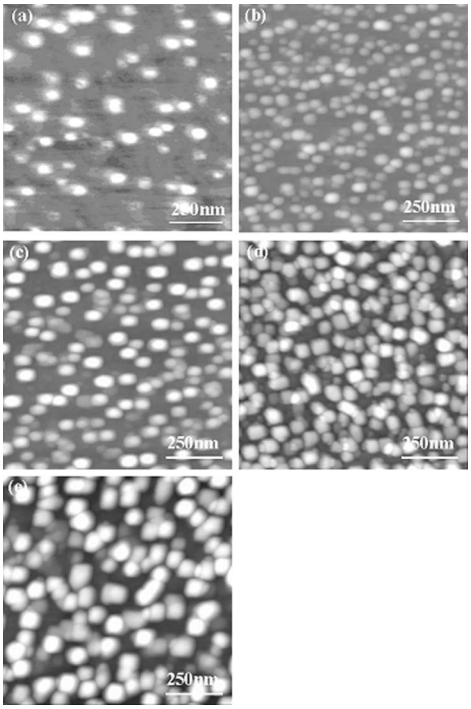

FIG. 7. The AFM images of samples A–E.

on the film surface. (2) With increasing the thickness of the LCMO film, the crystalline grains grow up and its crystalline quality becomes better. These results are reconfirmed by the measurements of the x-ray elasticity modulus, which will be published elsewhere. The average sizes of the grains are 24, 36, 45, and 50 nm and the densities of the grains are $1.82\times10^{10}/\mathrm{cm}^2$, $1.43\times10^{10}/\mathrm{cm}^2$, $1.5\times10^{10}/\mathrm{cm}^2$, and $1.27\times10^{10}/\mathrm{cm}^2$ for samples B, C, D, and E, respectively. Figure 7 shows the AFM images of the samples. Similar to the SEM results, one can see self-organized grains with a tetragonal shape on the surface. As expected, the sizes and densities of the grains are also similar to the SEM results. As mentioned above, the surface roughness of the five samples measured by AFM is highly consistent with that shown in Fig. 5.

The tetragonal crystalline morphology is the result of recrystallization during the annealing process and reflects that the deposition condition is of benefit to the formation of the crystalline grains. As well known, there exist a lattice mismatch and a thermal expansion coefficient mismatch between the LCMO film and the STO substrate. Our previous paper has reported that thermal expansion coefficient mismatch plays an important role in determining the surface morphology of the LCMO films when the thickness of the LCMO film is less than a critical value.[21] The occurrence of crystalline grains in the LCMO layer could relax the strains in the films. Therefore the crystalline grains are energetically favored and more stable than the corresponding two-dimensional pseudomorphic layer.

IV. CONCLUSION

The effects of thickness of LCMO film on its microstructures and morphology deposited on STO (001) single crystalline were studied by high-resolution x-ray diffraction (HXRD), x-ray reflection (XRR), GIXRD, SEM, and AFM methods. The results show that the LCMO films are well oriented in the $[00l]$ direction perpendicular to the substrate surface. Regular tetragonal crystalline grains are uniformly distributed on the film surface indicating the deposition condition being of benefit to the formation of the crystalline grains. With the increase of the film thickness, the crystalline quality of the LCMO film is improved, while the surface becomes rougher. There exists a nondesigned cap layer on the upper surface of the LCMO layer for all the samples. Further investigation to illustrate the relation between the structure and magnetic and transport properties of the LCMO film is in progress which will be published elsewhere.

ACKNOWLEDGMENTS

The work carried out in the University of Hong Kong has been supported by Research Grants Council (RGC) of Hong Kong (Project No. HKU7024/05P) and CRCG of the University of Hong Kong. The work done in the Institute of Physics, CAS was supported by the National Natural Science Foundation of China (Grant Nos. 10274096 and 10574159).

[1] H. D. Megaw and D. Helen, *Ferroelectricity in Crystals* (Methuen, London, 1957).
[2] J. G. Bednorz and K. A. Miller, Z. Phys. B: Condens. Matter **64**, 189 (1986).
[3] J. G. Bendnora, M. Takashige, and K. A. Muller, Europhys. Lett. **3**, 379 (1987).
[4] S. Jin, T. H. Tiefel, M. Mccormack, R. A. Fastnacht, R. Ramesh, and L. H. Chen, Science **264**, 413 (1994).
[5] S. Jin, T. H. Tiefel, M. Mccormack, H. M. Obryan, L. H. Chen, R. Ramesh, and D. Schurig, Appl. Phys. Lett. **67**, 557 (1995).
[6] E. E. Fullerton, M. J. Conover, J. E. Mattson, C. H. Sowers, and S. D. Bader, Appl. Phys. Lett. **63**, 1699 (1993).
[7] H. D. Megaw, Proc. R. Soc. London, Ser. A **189**, 261 (1947).
[8] N. Kistaedter *et al.*, Appl. Phys. Lett. **69**, 1226 (1996).
[9] W. J. Gallagher *et al.*, J. Appl. Phys. **81**, 3741 (1997).
[10] J. Jorzick, O. Demokritov, B. Hillebrands, B. Bartenlian, C. Chappert, D. Decanini, F. Rousseaux, and E. Cammbril, Appl. Phys. Lett. **75**, 3859 (1999).
[11] P. Schiffer, A. P. Ramirez, W. Bao, and S. W. Cheong, Phys. Rev. Lett. **75**, 3336 (1995).
[12] C. Zener, Phys. Rev. **82**, 403 (1951).
[13] R. A. Rao, D. Lavric, T. K. Nath, and C. B. Ecom, Appl. Phys. Lett. **85**, 4794 (1999).
[14] R. B. Praus, G. M. Gross, F. S. Razavi, and H. U. Habermeier, J. Magn. Magn. Mater. **211**, 41 (2000).
[15] M. Bibes *et al.*, J. Appl. Phys. **89**, 6686 (2001).
[16] J. Gao and F. X. Hu, Appl. Phys. Lett. **86**, 092504 (2005).
[17] G. Parrat, Phys. Rev. **95**, 359 (1954).
[18] G. M. Luo, M. L. Yan, Z. H. Mai, W. Y. Lai, and Y. T. Wang, Phys. Rev. B **56**, 3290 (1997).
[19] X. M. Chen *et al.*, Int. J. Mod. Phys. B **16**, 3439 (2002).
[20] W. X. Yu *et al.*, J. Phys. D **33**, 2363 (2000).
[21] X. M. Chen *et al.*, Mod. Phys. Lett. B **16**, 1049 (2002).